PHYSICAL REVIEW C **82**, 022501(R) (2010)

Double-β decay Q value of ^{150}Nd

V. S. Kolhinen,* T. Eronen, D. Gorelov, J. Hakala, A. Jokinen, A. Kankainen, I. D. Moore, J. Rissanen, A. Saastamoinen, J. Suhonen, and J. Äystö

Department of Physics, P. O. Box 35 (YFL), FI-40014 University of Jyväskylä, Finland

(Received 28 April 2010; published 18 August 2010)

The double-β decay Q value of ^{150}Nd was determined by using the JYFLTRAP Penning trap mass spectrometer. The measured mass difference between ^{150}Nd and ^{150}Sm is 3371.38(20) keV. This new value deviates by 3.7 keV from the previously adopted value of 3367.7(22) keV and is a factor of 10 more precise. Accurate knowledge of this Q value is important because ^{150}Nd is a primary candidate to be used in the search for neutrinoless double-β decay modes in several experiments.

DOI: 10.1103/PhysRevC.82.022501 PACS number(s): 21.10.Dr, 23.40.Bw, 27.30.+t

Experiments carried out on solar atmospheric accelerator and reactor neutrinos have provided evidence for neutrino oscillations and for a nonzero rest mass of neutrinos. From these data, one can extract the difference of squared masses of the neutrinos and the mixing angles [1–3]. However, these experiments do not provide information on the absolute mass scale of the neutrinos, nor do they give information toward answering the question of whether the neutrino is a Dirac or a Majorana particle. A Majorana neutrino is identical to its antiparticle and, thus, violates lepton-number conservation. The only feasible way to answer these questions is via neutrinoless double-β decay ($0\nu\beta\beta$) experiments. Observation of this process would be unquestionable evidence of the Majorana nature of neutrinos and, furthermore, would provide definitive proof of new physics beyond the standard model, which supports the concept of a neutrino as a massless Dirac particle. The mass of a Majorana neutrino is then inversely proportional to the double-β decay half-life [4].

^{150}Nd is considered to be one of the most promising candidates in the search for neutrinoless double-β decay because the relatively high value of the decay energy $Q_{\beta\beta} =$ 3367.7(22) keV [5], is above the majority of background β-decay energies. Additionally, ^{150}Nd has been successfully used in time-projection-chamber experiments [6,7]. Moreover, three major future experiments, the Drift Chamber Beta-ray Analyzer (DCBA) [8], SuperNEMO [9], and SNO+ [10], plan to use this material. Therefore, accurate knowledge of the mass difference between ^{150}Nd and its double-β decay daughter ^{150}Sm is important for these experiments. A precise mass difference measurement directly impacts on the search for the $0\nu\beta\beta$ peak by narrowing the energy window in the two-electron spectrum.

The $Q_{\beta\beta}$ measurement was performed at the IGISOL facility [11,12] in the Accelerator Laboratory of the University of Jyväskylä, Finland, by using an electric discharge ion source inside the ion-guide system. Ions were created by applying a voltage between two electrodes, which contain natural neodymium and samarium, which evaporate material into helium gas at a pressure of 2–4 mbar. Gas flow extracted the ions from the electric discharge source into a sextupole ion guide [13], whereby they were guided into a differential pumping stage and were accelerated up to $30q$-keV energy. This continuous beam was mass separated by using a 55° dipole magnet with mass resolving power on the order of $M/\Delta M \approx 500$ for singly charged ions. The isobar $A = 150$ and $q = 1$ were selected with the magnet and were transported through the electrostatic switchyard, were decelerated, and were injected into a radio-frequency quadrupole cooler/buncher [14]. In this device, the ions were cooled, were accumulated, and were bunched before injection into the double Penning trap spectrometer JYFLTRAP [15]. A schematic of the experimental setup is shown in Fig. 1, by illustrating the ion guide, beam line components, and JYFLTRAP.

The JYFLTRAP spectrometer consists of two identical cylindrical Penning traps housed inside one 7-T superconducting solenoid. The first trap, the purification trap, operates in a low-pressure helium buffer gas environment and is used for isobaric cleaning by means of a buffer gas-cooling technique [16]. The second Penning trap, the precision trap, is used for the measurement of the cyclotron frequency of the ions of interest $\nu_c = \frac{1}{2\pi}\frac{q}{m}B$ by applying a time-of-flight (TOF) ion-cyclotron resonance technique [17,18].

The cyclotron frequency difference of ^{150}Nd$^+$ and the double-β decay daughter ^{150}Sm$^+$ in a 7-T field is about 17 Hz, which is large enough for separation in the purification trap [15]. However, to improve the quality of the resonances, the purification trap was tuned to have poorer resolution but better centering of the ions. The complete separation of the two species was accomplished in another cleaning step [19], whereby contaminant ions were excited in the precision trap into a large orbit. The ions were subsequently retransferred to the purification trap through a 2-mm diameter channel, which only allows for the ions of interest to survive. After an additional cooling and centering in the purification trap, they were transferred to the precision trap for cyclotron frequency determination.

The mass measurement was performed by scanning the sideband frequency of the ions of interest $\nu_+ + \nu_-$, where ν_+ and ν_- are the reduced cyclotron frequency and the magnetron frequency, respectively. When the excitation frequency matches the sum frequency $\nu_+ + \nu_-$, which is the true

*veli.kolhinen@jyu.fi

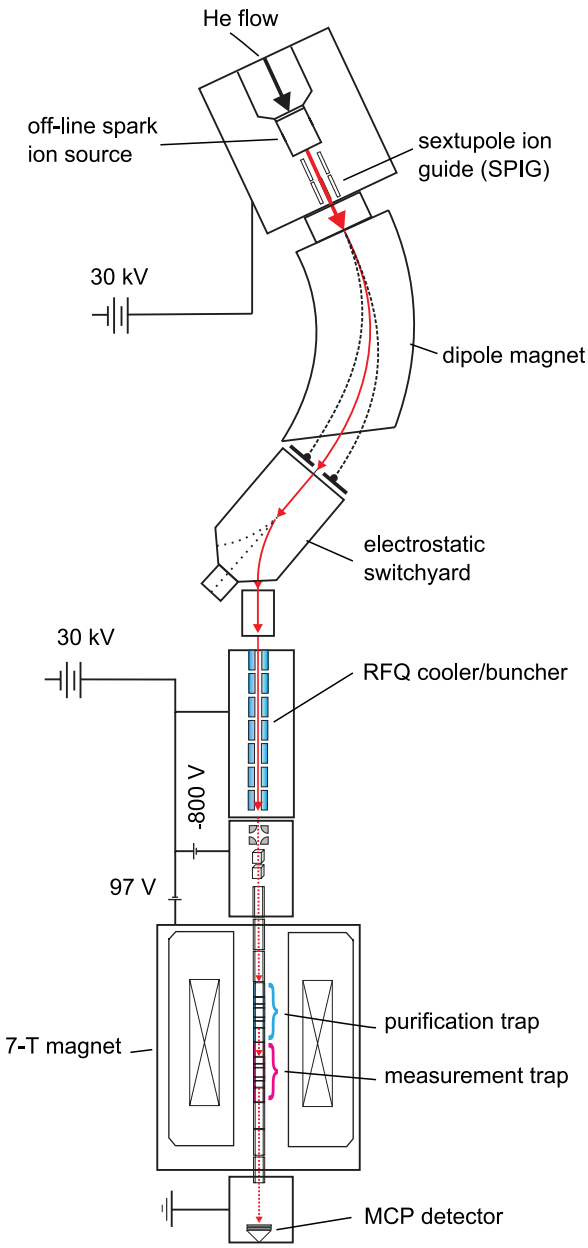

FIG. 1. (Color online) Schematic of the JYFLTRAP beam line.

cyclotron frequency ν_c in an ideal Penning trap, a maximal periodic conversion between the magnetron and the reduced cyclotron motion occurs [20]. After one full conversion to the reduced cyclotron motion, the radial energy of the ions reaches a maximum, which leads to a stronger acceleration of the ions as they are extracted through the gradient of the magnetic field. This reduces the flight time of the ions from the trap to a microchannel plate detector (MCP).

A Ramsey-type ion motion excitation scheme [21,22] was applied by allowing for better precision in the cyclotron frequency determination. The duration of the excitation used was two 25-ms fringes separated by a waiting period of 350 or 750 ms. A longer waiting time between fringes results in narrower resonances; however, it increases the interaction time between the ions and the residual gas in the measurement trap, which causes velocity damping. This, in turn, results in a wider TOF distribution of ions. In the studied mass range, such damping did not have an effect on resonance shape itself, although it might have caused larger uncertainties than expected, especially when relatively small magnetron amplitudes were applied in the measurement trap.

Measurements were carried out by scanning one cycle of ^{150}Nd followed by another cycle of ^{150}Sm and by repeating this pattern. One cycle lasted approximately 1 min. In this manner, the shift in the frequency ratio caused by the magnetic-field drift was minimized. In the analysis, the data were divided into 15-cycle-long intervals, and each set was analyzed independently. Figure 2 shows an example of resonances of both ^{150}Nd and ^{150}Sm, respectively. To avoid count-rate-dependent shifts in the cyclotron frequency, a count-rate class analysis was applied [23]. In this method, each 15-cycle-long interval was divided into classes according to the number of detected ions, and each class was fitted separately. A linear fit was applied to the data, and the final result was obtained by extrapolating to 0.6, which is estimated to correspond to a single ion in the

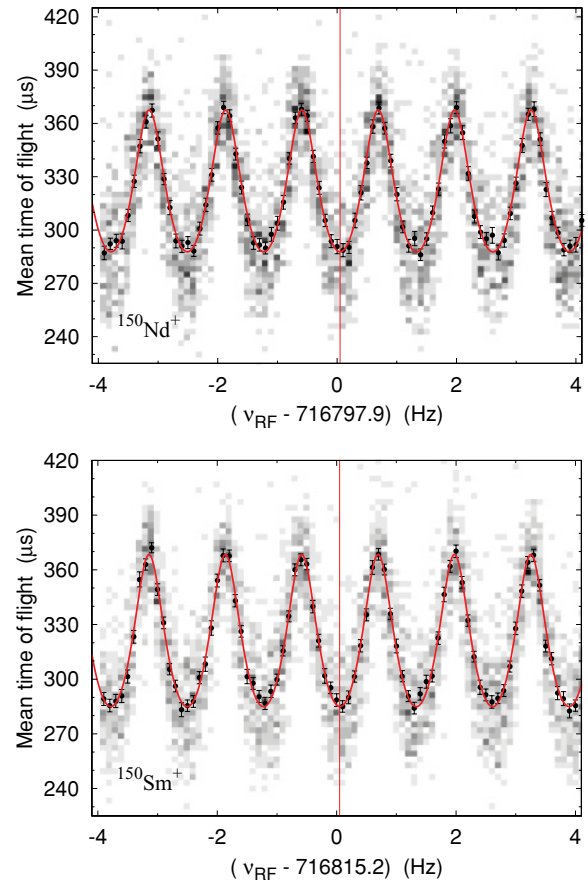

FIG. 2. (Color online) TOF ion-cyclotron resonances of ^{150}Nd$^+$ and ^{150}Sm$^+$ with a (25-750-25 ms) Ramsey excitation pattern, which contains 15 scan cycles with settings A (detailed in Table I). Shadowed boxes show the density of detected ions (the darker the pixel, the more ions it represents), black dots are the average TOFs with corresponding uncertainties, and the solid (red) line is the fitted line shape.

TABLE I. Summary of all measurements. Different excitation times, magnetron amplitudes in the measurement trap, extraction voltages, and transfer times from the purification trap to the measurement trap were used. (A) 25-750-25 ms, $A(\nu_-) = 60$ mV, $U = -1400$ V. (B) 25-350-25 ms, $A(\nu_-) = 60$ mV, $U = -1400$ V. (C) 25-350-25 ms, $A(\nu_-) = 60$ mV, $U = -1200$ V. (D) 25-750-25 ms, $A(\nu_-) = 50$ mV, $U = -1600$ V. (E) 25-350-25 ms, $A(\nu_-) = 60$ mV, $U = -1600$ V. (F) 25-750-25 ms, $A(\nu_-) = 60$ mV, $U = -1600$ V, transfer time + 0.3 μs.

Set	Number of scans	Frequency ratio $\frac{\nu_{c,\mathrm{Sm}}}{\nu_{c,\mathrm{Nd}}}$	Q value (keV)
A	255	1.000 024 1422(23)	3371.37(32)
B	105	1.000 024 1396(41)	3371.01(58)
C	45	1.000 024 1379(70)	3370.78(98)
D	195	1.000 024 1428(40)	3371.46(55)
E	105	1.000 024 1432(34)	3371.51(48)
F	120	1.000 024 1446(43)	3371.71(55)
Average		1.000 024 1423(14)	3371.38(20)

measurement trap, which assumes 60% detection efficiency for the MCP.

The Q value was calculated with the relation,

$$Q = m_m - m_d = \left(\frac{\nu_{c,\mathrm{Sm}}}{\nu_{c,\mathrm{Nd}}} - 1\right)(m_{\mathrm{Sm}} - m_e) + \frac{\nu_{c,\mathrm{Sm}}}{\nu_{c,\mathrm{Nd}}} B_{e,\mathrm{Sm}} - B_{e,\mathrm{Nd}}, \quad (1)$$

where $\nu_{c,\mathrm{Sm}}$ and $\nu_{c,\mathrm{Nd}}$ are the measured cyclotron frequencies for singly charged ^{150}Sm and ^{150}Nd ions, m_{Sm} is the mass of a ^{150}Sm atom, m_e is the mass of an electron, and $B_{e,\mathrm{Sm}}$ and $B_{e,\mathrm{Nd}}$ are the first atomic electron-binding energies. The values used were as follows: the mass excess $ME_{\mathrm{Sm}} = -77\,057.3(2.4)$ keV [5], $m_e = 510.998\,910(13)$ keV [24], $B_{e,\mathrm{Sm}} = 5.6437$ eV, $B_{e,\mathrm{Nd}} = 5.5250$ eV [25], and the atomic mass unit $u = 931\,494.0090(71)$ keV [26].

During the experiment, different settings were used when applying the 25-750-25 ms and the 25-350-25 ms (on-off-on) excitation patterns. Three extraction voltages (U) were applied to the last electrode before the 30-keV acceleration: -1400 V in sets A and B, -1200 V in set C, and -1600 V in sets D–F. In set C, a moderate frequency dependence in the count rate was observed; and, therefore, the set was only measured for 45 rounds. Nevertheless, this did not affect the average TOF of the ions, and the extracted Q value agrees with that from the other sets. Therefore, the data were kept in the analysis. The results are shown in Table I. Birge ratio ≈ 1 [27] in each set except in set D where it was 0.8, which shows that deviation in the data is purely statistical, and, in set D, the fitting uncertainties were too large compared to the deviations around the average value. The average Q value was calculated by taking a weighted average of all values, which results in a final Q value of 3371.38(20) keV. Figure 3 shows the measured frequencies and the obtained Q values in set A.

The new accurate Q-value measurement will directly influence the energy region of interest in which the next-generation underground experiments expect to locate the weak peak attributed to the ($0\nu\beta\beta$) decay. Therefore, it is of interest to study the prospects of determining the neutrino mass in

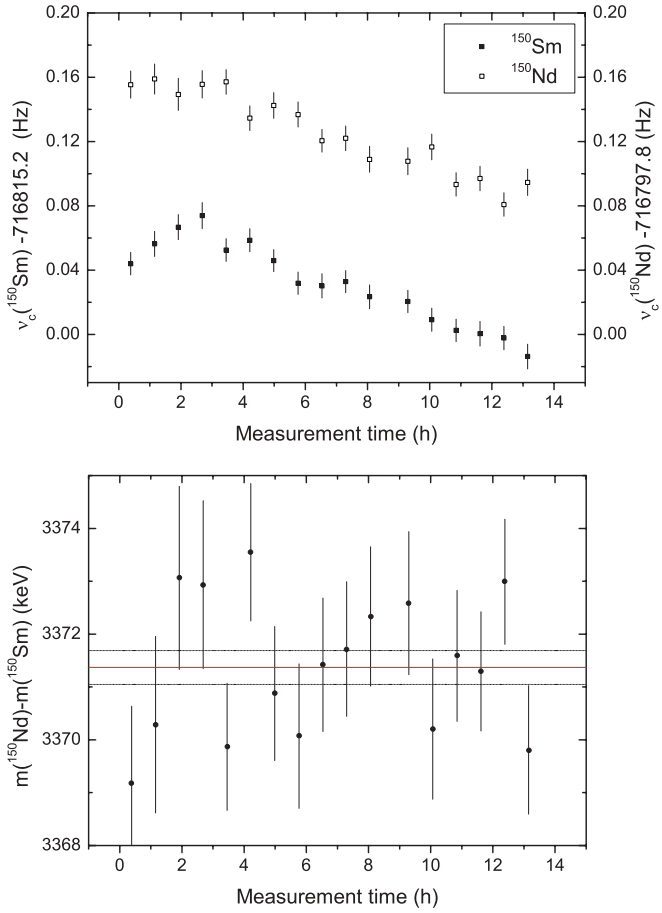

FIG. 3. (Color online) Top: Series of extracted cyclotron frequencies for ^{150}Nd and ^{150}Sm obtained by using a 25-750-25-ms Ramsey excitation pattern with the parameter set A as detailed in Table I. Each data point contains 15 cycles. Bottom: Mass difference of ^{150}Nd and ^{150}Sm obtained from frequencies taken from the top panel. Solid (red) line shows the average of 3371.37 keV. The dotted black lines denote one standard deviation of $\sigma = 0.32$ keV.

these experiments. By assuming that the $0\nu\beta\beta$ decay proceeds mainly through the neutrino mass and that the $0\nu\beta\beta$ decay of ^{150}Nd is detected, the measured half-life can be connected with the (effective) neutrino mass $\langle m_\nu \rangle$ through the relation,

$$\left[t_{1/2}^{(0\nu)}\right]^{-1} = G^{(0\nu)}(M^{(0\nu)})^2\langle m_\nu \rangle^2 , \quad (2)$$

where $G^{(0\nu)}$ is the lepton phase-space factor defined such that it absorbs the electron rest-mass term m_e^{-2}. The quantity $M^{(0\nu)}$ is the nuclear matrix element [28]. The effective neutrino mass is a linear combination of the neutrino-mass eigenstates weighted by the Majorana CP phases and the elements of the neutrino mixing matrix [28]. The measured values of the elements of the mixing matrix, together with the unknown CP phases, define regions of the allowed values of $\langle m_\nu \rangle$. Although for the *normal* neutrino-mass hierarchy, $\langle m_\nu \rangle$ can be zero, for the *inverted* and *degenerate* mass hierarchies $\langle m_\nu \rangle$ only attain finite values above a few tens of millielectron volts [4].

The nuclear matrix element in Eq. (2) has only been computed in a few models [29–31] that take the nuclear deformation of the $0\nu\beta\beta$ mother and daughter nuclei ^{150}Nd

TABLE II. Values of the auxiliary quantities of Eqs. (3) and (4) for three different models of deformed nuclei.

Quantity	P-SU(3)	PHFB	IBM-2
$C^{(0\nu)}$	13.5	10.4	5.68
$T_{0.02}$	3.38	2.60	1.42

and ^{150}Sm, respectively, into account. In Ref. [29], the pseudo-SU(3) [P-SU(3)] deformed model was used, in Ref. [30], the projected Hartree-Fock-Bogoliubov (PHFB) mean-field approach was adopted, and in Ref. [31], the interacting boson-fermion model (IBM-2) was applied. By using the Q value of the present experiment and the machinery of Ref. [28], one can evaluate the involved phase-space integral and can rewrite the $0\nu\beta\beta$-decay half-life of Eq. (2) for ^{150}Nd as

$$t_{1/2}^{(0\nu)} \leqslant \langle m_\nu \rangle^{-2} C^{(0\nu)} \times 10^{23} \text{ yr}, \tag{3}$$

where $\langle m_\nu \rangle$ is given in units of electron volts and the auxiliary factor $C^{(0\nu)}$ is given in Table II for the three mentioned nuclear models. Under the assumption that the neutrino mass obeys the inverted (or degenerate) hierarchy, one can derive the following limits for the $0\nu\beta\beta$ half-life of ^{150}Nd:

$$1.8 \times 10^{22} \text{ yr} < t_{\text{inverted}}^{(0\nu)} < T_{0.02} \times 10^{27} \text{ yr}. \tag{4}$$

The lower limit (at 90% confidence level) comes from the recent measurement of the NEMO-3 detector [32], and the upper limit comes from the use of the relation Eq. (3) with $\langle m_\nu \rangle \gtrsim 0.02$ eV [4]. The quantity $T_{0.02}$ has been listed in Table II for the three nuclear models.

It should be noted that the values of the phase-space factor $G^{(0\nu)}$ and the nuclear matrix element $M^{(0\nu)}$ in Eq. (2) depend on the value of the axial-vector coupling constant g_A [28]. We have $G^{(0\nu)} \propto g_A^4$ and $M^{(0\nu)} = M_{\text{GT}}^{(0\nu)} - (g_V/g_A)^2 M_F^{(0\nu)}$, where $g_V = 1.00$ is the vector-coupling constant. The exact value of g_A is unknown in heavy nuclei. Both the bare value $g_A = 1.25$ and the quenched value $g_A = 1.00$ have been used in $0\nu\beta\beta$ calculations [4,29–31,33–35]. For the evaluation of the right-hand side of Eq. (3), we have used $g_A = 1.00$, since it gives the most conservative (highest) upper limits for $C^{(0\nu)}$ within the range $1.0 \leqslant g_A \leqslant 1.25$. The next-generation $0\nu\beta\beta$ experiments have good potential to reach the upper limits indicated in Eq. (4), obtained from Eq. (3) by taking $\langle m_\nu \rangle \gtrsim 0.02$ eV.

To conclude, we have greatly improved the accuracy of the Q value of the neutrinoless double-β decay of ^{150}Nd by using the JYFLTRAP Penning trap. This accurate value is needed to pinpoint the $0\nu\beta\beta$ peak in the two-electron energy spectrum in the present and future underground experiments, which search for the Majorana-neutrino mass. The next-generation $0\nu\beta\beta$ setups have good potential to detect the neutrinoless double-β decay of ^{150}Nd provided that the decay proceeds mainly via the Majorana mass, which obeys either the degenerate or the inverted mass hierarchy.

This work was supported by the Academy of Finland under the Finnish Center of Excellence Programme 2006-2011 (Project No. 213503, Nuclear and Accelerator Based Physics Programme at JYFL). We thank Raimo Seppälä for help with the Nd and Sm materials.

[1] M. Maltoni *et al.*, New J. Phys. **6**, 122 (2004).
[2] T. Schwetz, M. Tórtola, and J. W. F. Valle, New J. Phys. **10**, 113011 (2008).
[3] H. Nunokawa, S. Parke, and J. W. F. Valle, Prog. Part. Nucl. Phys. **60**, 338 (2008).
[4] F. T. Avignone III, S. R. Elliott, and J. Engel, Rev. Mod. Phys. **80**, 481 (2008).
[5] G. Audi, A. H. Wapstra, and C. Thibault, Nucl. Phys. A **729**, 337 (2003).
[6] A. De Silva, M. K. Moe, M. A. Nelson, and M. A. Vient, Phys. Rev. C **56**, 2451 (1997).
[7] R. Arnold *et al.*, Nucl. Instrum. Methods Phys. Res. A **536**, 79 (2005).
[8] N. Ishihara *et al.*, J. Phys.: Conf. Series **203**, 012071 (2010).
[9] F. Piquemal, Phys. At. Nucl. **69**, 2096 (2006).
[10] K. Zuber, AIP Conf. Proc. **942**, 101 (2007).
[11] J. Äystö, Nucl. Phys. A **693**, 477 (2001).
[12] H. Penttilä *et al.*, Eur. Phys J. A **25** (Suppl. 1), 745 (2005).
[13] P. Karvonen *et al.*, Nucl. Instrum. Methods Phys. Res. B **266**, 4794 (2008).
[14] A. Nieminen *et al.*, Nucl. Instrum. Methods Phys. Res. A **469**, 244 (2001).
[15] V. S. Kolhinen *et al.*, Nucl. Instrum. Methods Phys. Res. A **528**, 776 (2004).
[16] G. Savard *et al.*, Phys. Lett. A **158**, 247 (1991).
[17] G. Gräff, H. Kalinowsky, and J. Traut, Z. Phys. A **297**, 35 (1980).
[18] M. König *et al.*, Int. J. Mass Spectrom. **142**, 95 (1995).
[19] T. Eronen *et al.*, Nucl. Instrum. Methods Phys. Res. B **266**, 4527 (2008).
[20] L. S. Brown and G. Gabrielse, Rev. Mod. Phys. **58**, 233 (1986).
[21] S. George *et al.*, Int. J. Mass Spectrom. **264**, 110 (2007).
[22] M. Kretzschmar, Int. J. Mass Spectrom. **264**, 122 (2007).
[23] A. Kellerbauer *et al.*, Eur. Phys. J. D **22**, 53 (2003).
[24] C. Amsler *et al.* (Particle Data Group), Phys. Lett. B **667**, 103 (2008).
[25] NIST Chemistry WebBook, edited by P. J. Linstrom and W. G. Mallard, [http://webbook.nist.gov].
[26] G. Audi, Hyperfine Interact. **132**, 7 (2001).
[27] R. T. Birge, Phys. Rev. **40**, 207 (1932).
[28] J. Suhonen and O. Civitarese, Phys. Rep. **300**, 123 (1998).
[29] J. G. Hirsch, O. Castaños, and P. O. Hess, Nucl. Phys. A **582**, 124 (1995).
[30] K. Chaturvedi, R. Chandra, P. K. Rath, P. K. Raina, and J. G. Hirsch, Phys. Rev. C **78**, 054302 (2008).
[31] J. Barea and F. Iachello, Phys. Rev. C **79**, 044301 (2009).
[32] J. Argyriades *et al.*, Phys. Rev. C **80**, 032501(R) (2009).
[33] F. Šimkovic, A. Faessler, V. Rodin, P. Vogel, and J. Engel, Phys. Rev. C **77**, 045503 (2008).
[34] M. Kortelainen and J. Suhonen, Phys. Rev. C **76**, 024315 (2007).
[35] J. Suhonen and M. Kortelainen, Int. J. Mod. Phys. E **17**, 1 (2008).